SANDIA REPORT

SAND2017-10078
Unlimited Release
Printed September 2017

Electromagnetic Pulse Excitation of Finite-Long Dissipative Conductors over a Conducting Ground Plane in the Frequency Domain

Salvatore Campione, Larry K. Warne, Richard L. Schiek, Lorena I. Basilio

Prepared by
Sandia National Laboratories
Albuquerque, New Mexico 87185 and Livermore, California 94550

Sandia National Laboratories is a multimission laboratory managed and operated by National Technology and Engineering Solutions of Sandia, LLC., a wholly owned subsidiary of Honeywell International, Inc., for the U.S. Department of Energy's National Nuclear Security Administration under contract DE-NA-0003525.

Approved for public release; further dissemination unlimited.

Issued by Sandia National Laboratories, operated for the United States Department of Energy by Sandia Corporation.

NOTICE: This report was prepared as an account of work sponsored by an agency of the United States Government. Neither the United States Government, nor any agency thereof, nor any of their employees, nor any of their contractors, subcontractors, or their employees, make any warranty, express or implied, or assume any legal liability or responsibility for the accuracy, completeness, or usefulness of any information, apparatus, product, or process disclosed, or represent that its use would not infringe privately owned rights. Reference herein to any specific commercial product, process, or service by trade name, trademark, manufacturer, or otherwise, does not necessarily constitute or imply its endorsement, recommendation, or favoring by the United States Government, any agency thereof, or any of their contractors or subcontractors. The views and opinions expressed herein do not necessarily state or reflect those of the United States Government, any agency thereof, or any of their contractors.

Printed in the United States of America. This report has been reproduced directly from the best available copy.

Available to DOE and DOE contractors from
U.S. Department of Energy
Office of Scientific and Technical Information
P.O. Box 62
Oak Ridge, TN 37831

Telephone: (865) 576-8401
Facsimile: (865) 576-5728
E-Mail: reports@osti.gov
Online ordering: http://www.osti.gov/scitech

Available to the public from
U.S. Department of Commerce
National Technical Information Service
5301 Shawnee Rd
Alexandria, VA 22312

Telephone: (800) 553-6847
Facsimile: (703) 605-6900
E-Mail: orders@ntis.gov
Online order: http://www.ntis.gov/search

SAND2017-10078
Unlimited Release
Printed September 2017

Electromagnetic Pulse Excitation of Finite-Long Dissipative Conductors over a Conducting Ground Plane in the Frequency Domain

Salvatore Campione, Larry K. Warne, and Lorena I. Basilio
Electromagnetic Theory

Richard L. Schiek
Electrical Models & Simulations

Sandia National Laboratories
P.O. Box 5800
Albuquerque, New Mexico 87185-1152

Abstract

This report details the modeling results for the response of a finite-length dissipative conductor interacting with a conducting ground to a hypothetical nuclear device with the same output energy spectrum as the Fat Man device. We use a frequency-domain method based on transmission line theory and implemented it in a code we call ATLOG – Analytic Transmission Line Over Ground. Select results are compared to ones computed using the circuit simulator Xyce.

Intentionally Left Blank

ACKNOWLEDGMENTS

The authors acknowledge valuable discussions with Dr. Keith L. Cartwright, Org. 1352 and Eric Nelson from Los Alamos National Laboratories. Also, the authors acknowledge Jeff Bull and Scott Smith from Los Alamos National Laboratories for conducting the environment calculations.

Contents

FIGURES

Intentionally Left Blank

1. INTRODUCTION

The purpose of this report is to provide results for the current induced on finite-length dissipative conductors interacting with a conducting ground, when excited by source region electromagnetic pulse (SREMP) coming from a hypothetical nuclear device with the same output energy spectrum as the Fat Man device [1]. We will make use of a frequency-domain method based on transmission line theory and implemented it in a code we call ATLOG – Analytic Transmission Line Over Ground [2, 3], which has been previously compared to EMPHASIS [4] and CST Microwave Studio [5] full-wave simulations. These results have compared favorably as reported in [2]. For completeness, we summarize the ATLOG model in Section 2, and then proceed with the description of a finite-wire under the SREMP in the remainder of this report. This drive waveform is being used here as an example of nuclear-weapon output; the theoretical model and ATLOG code are general and can be used to characterize transmission-line output for any pulse waveform.

2. ATLOG MODEL FOR A CONDUCTING WIRE OVER A GROUND PLANE EXCITED BY A PLANE WAVE

2.1. Definition of transmission line parameters

The coupling to the transmission line mode from an incident plane wave is considered. This is the same calculation as carried out previously in [2, 3] and references therein and is reproduced here for convenience. The transmission line equations are

$$\frac{dV}{dz} = -ZI + E_z^{\text{inc}}, \qquad \frac{dI}{dz} = -YV. \tag{1}$$

In Eq. (1), the impedance is defined as $Z = Z_0 + Z_2 + Z_4$, where (taking an $\exp(j\omega t)$ time dependence)

$$Z_0 = \begin{cases} \omega\dfrac{\mu_0}{2\pi}\dfrac{1}{(1-j)a/\delta} & \delta/a < 1/10 \\ j\omega\dfrac{\mu_0}{8\pi} + \dfrac{1}{\sigma_0\pi a^2} & \delta/a > 10 \\ -j\omega\dfrac{\mu_0}{2\pi(1-j)a/\delta}\dfrac{J_0((1-j)a/\delta)}{J_1((1-j)a/\delta)} & \text{otherwise} \end{cases} \tag{2}$$

$$Z_2 = \begin{cases} j\omega\dfrac{\mu_0}{2\pi}\ln(b/a) + j\omega\dfrac{\mu_0}{2\pi}\ln\left(\dfrac{h}{b} + \sqrt{\left(\dfrac{h}{b}\right)^2 - 1}\right) & h \geq b \\ j\omega\dfrac{\mu_0}{2\pi}\ln(b/a) & h < b \end{cases} \tag{3}$$

$$Z_4 = \begin{cases} j\omega\mu_0\dfrac{H_0^{(2)}(k_4 h)}{2\pi k_4 h H_1^{(2)}(k_4 h)} & h \geq b \\ j\omega\mu_0\dfrac{H_0^{(2)}(k_4 b)}{2\pi k_4 b H_1^{(2)}(k_4 b)} & h < b \end{cases} \tag{4}$$

with $k_4^2 = \omega\mu_0(\omega\varepsilon_4 - j\sigma_4)$, $\delta = \sqrt{\dfrac{2}{\omega\mu_0\sigma_0}}$ and where ε_4 is the ground permittivity, σ_4 is the ground conductivity, σ_0 is the wire conductivity, a is the wire radius, b is the radius of a dielectric shell coating the wire, and h is the distance of the transmission line from the conducting ground plane.

The admittance is defined as $\frac{1}{Y}=\frac{1}{Y_e}+\frac{1}{Y_4}$ with $Y_e=G_e+j\omega C_e$ and

$$\frac{1}{C_e}=\begin{cases}\sqrt{\left(\frac{h/h_e}{C_0}+\frac{1}{C_2}\right)^2-\left(\frac{b/h_e}{C_0}+\frac{A_2}{C_2}\right)^2} & h>b\\ \frac{1}{C_2}\sqrt{(1-A_2)\left(1+A_2+\frac{C_2}{\pi\varepsilon_0}\right)} & h=b\\ \frac{1}{C_2} & h<-b\end{cases} \tag{5}$$

where $h_e=\sqrt{h^2-b^2}$, $C_2=\frac{2\pi\varepsilon_2}{\ln(b/a)}$, ε_2 is the permittivity of a dielectric shell coating the wire, $A_2=0.7(1-a/b)(1-h_e/h)\frac{\varepsilon_2-\varepsilon_0}{\varepsilon_2+\varepsilon_0}$, $C_0=\frac{2\pi\varepsilon_0}{\ln\left(h/b+\sqrt{(h/b)^2-1}\right)}$, $G_e=\frac{2\pi\sigma_{\text{air}}}{\ln(2h/b)}$ for $h>>b$, σ_{air} is the air conductivity, and

$$Y_4=\begin{cases}j\pi(\omega\varepsilon_4-j\sigma_4)k_4h\frac{H_1^{(2)}(k_4h)}{H_0^{(2)}(k_4h)} & h\geq b\\ j2\pi(\omega\varepsilon_4-j\sigma_4)k_4b\frac{H_1^{(2)}(k_4b)}{H_0^{(2)}(k_4b)+H_0^{(2)}\left(k_4\sqrt{4h^2+b^2}\right)e^{-jk_4\left(\sqrt{4h^2+b^2}-b\right)}} & h<-b\end{cases} \tag{6}$$

The case of a wire that is only partially buried $-b<h<b$ is not considered here.

2.2. ATLOG case to model finite lines

Consider the case of a finite wire in Figure 1. We consider the transmission line equations (1), for which eliminating the voltage gives

$$\left(\frac{d^2}{dz^2}-\gamma_L^2\right)I=-YE_z^{\text{inc}} \tag{7}$$

where $\gamma_L^2=ZY$. The solution of Eq. (7) is given by

$$\begin{aligned}I(z)&=[K_1+P(z)]e^{-\gamma_L z}+[K_2+Q(z)]e^{\gamma_L z}\\ V(z)&=\sqrt{\frac{Z}{Y}}\{[K_1+P(z)]e^{-\gamma_L z}-[K_2+Q(z)]e^{\gamma_L z}\},\end{aligned} \tag{8}$$

with $P(z)=\frac{1}{2}\sqrt{\frac{Y}{Z}}\int_{z_-}^{z} e^{\gamma_L z} E_z^{\text{inc}}(z)dz$ and $Q(z)=\frac{1}{2}\sqrt{\frac{Y}{Z}}\int_{z}^{z_+} e^{-\gamma_L z} E_z^{\text{inc}}(z)dz$. In the case where h is sizable compared with b, we have to include voltage sources at the ends of the line due to the incident plus reflected transverse electric fields (the current is not changed by these sources in the open-circuited case). In particular, the total voltage at the end of the lines z_- and z_+ (where $z_- < z < z_+$) is given by $V_t(z_\pm)=\pm I(z_\pm)Z_L^\pm = V(z_\pm)-V_0(z_\pm)$, with $V_0(z_\pm)=\left[E_x^{inc}(z_\pm)+E_x^{ref}(z_\pm)\right]h_e$. The constants in Eq. (8) are determined from the terminating impedances Z_L^- and Z_L^+ to the transmission line (at locations z_- and z_+, respectively). More specifically,

$$K_1=\rho_- e^{\gamma_L z_-}\frac{\rho_+ P(z_+)e^{-\gamma_L z_+}-Q(z_-)e^{\gamma_L z_+}}{e^{\gamma_L(z_+-z_-)}-\rho_-\rho_+ e^{-\gamma_L(z_+-z_-)}}+\frac{\rho_- V_0(z_+)e^{\gamma_L z_-}\Big/\left(\sqrt{\frac{Z}{Y}}+Z_L^+\right)+V_0(z_-)e^{\gamma_L z_+}\Big/\left(\sqrt{\frac{Z}{Y}}+Z_L^-\right)}{e^{\gamma_L(z_+-z_-)}-\rho_-\rho_+ e^{-\gamma_L(z_+-z_-)}}$$

$$K_2=\rho_+ e^{-\gamma_L z_+}\frac{\rho_- Q(z_-)e^{\gamma_L z_-}-P(z_+)e^{-\gamma_L z_-}}{e^{\gamma_L(z_+-z_-)}-\rho_-\rho_+ e^{-\gamma_L(z_+-z_-)}}-\frac{\rho_+ V_0(z_-)e^{-\gamma_L z_+}\Big/\left(\sqrt{\frac{Z}{Y}}+Z_L^-\right)+V_0(z_+)e^{-\gamma_L z_-}\Big/\left(\sqrt{\frac{Z}{Y}}+Z_L^+\right)}{e^{\gamma_L(z_+-z_-)}-\rho_-\rho_+ e^{-\gamma_L(z_+-z_-)}}, \quad (9)$$

where the reflection coefficients at positions z_- and z_+ are $\rho_-=\frac{Z_L^- - \sqrt{\frac{Z}{Y}}}{Z_L^- + \sqrt{\frac{Z}{Y}}}$ and $\rho_+=\frac{Z_L^+ - \sqrt{\frac{Z}{Y}}}{Z_L^+ + \sqrt{\frac{Z}{Y}}}$.

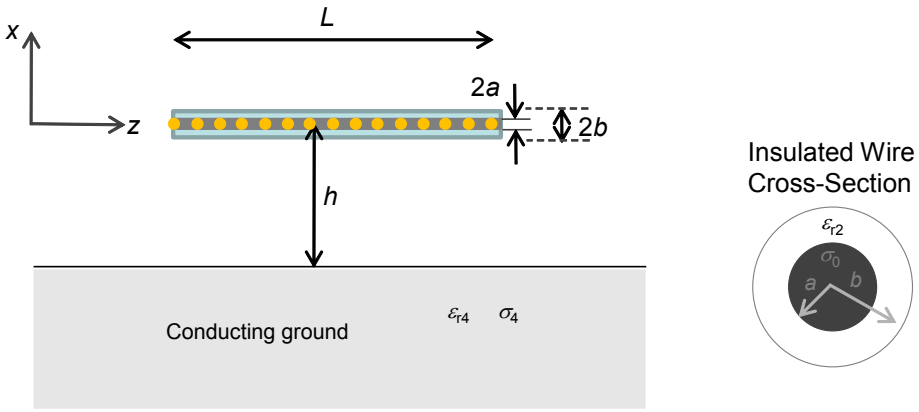

Figure 1. Schematic of the problem: a finite (coated) conducting wire with length *L* is located at a distance *h* from a conducting ground plane. The wire is illuminated by an experimental field distribution along its length at the sampled points indicated by orange circles. The inset shows the wire cross section.

3. EMP WAVEFORM DRIVE CONSIDERED IN THIS REPORT

In this section we report the time-domain profile of the SREMP excitation. This is the EMP drive that we will consider in the subsequent results section. As shown in Figure 1, the wire is illuminated by an experimental field distribution along its length at the sampled points indicated by orange circles. We have two sets of time series data: 1) the probes are spaced evenly at 20 m intervals from 0 m to 10 km; 2) the probes are spaced evenly at 2 m intervals from 0 m to 1 km.

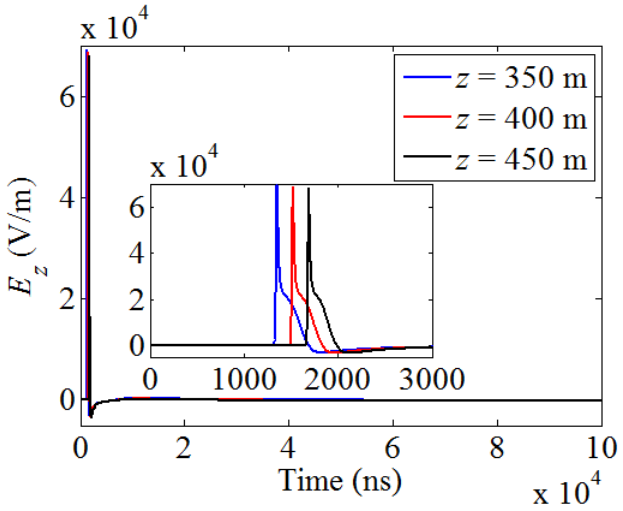

Figure 2. The *z*-component of the electric field versus time at three positions along the wire. The inset shows a zoom at early times.

We will first focus on the second set, and in particular on the data between 350 m and 450 m (the first set will be used in a later section). The time dependence of the field exciting the wire is reported in Figure 2. We want to double check the correctness of the free-space delay – given as $\Delta t = \Delta z / c$, equal to 166.67 ns after 50 m and 333.33 ns after 100 m. The peak of the blue curve is observed at 1357 ns. The peak of the red curve is observed at 1522 ns, about 165 ns delayed with respect to the blue curve. The peak of the black curve is observed at 1693 ns, about 336 ns delayed with respect to the blue curve.

Since the time-domain data is in accordance with the free-space delay, we Fourier transform the pulse in MATLAB to obtain its spectrum. This frequency-domain profile is shown in Figure 3(a) and will be used as input for ATLOG. We further inverse Fourier transform such spectrum with a FORTRAN code to guarantee correct manipulation of the data, and overlap the result to the time-domain data in Figure 3(b). The agreement between the original and the manipulated data is good.

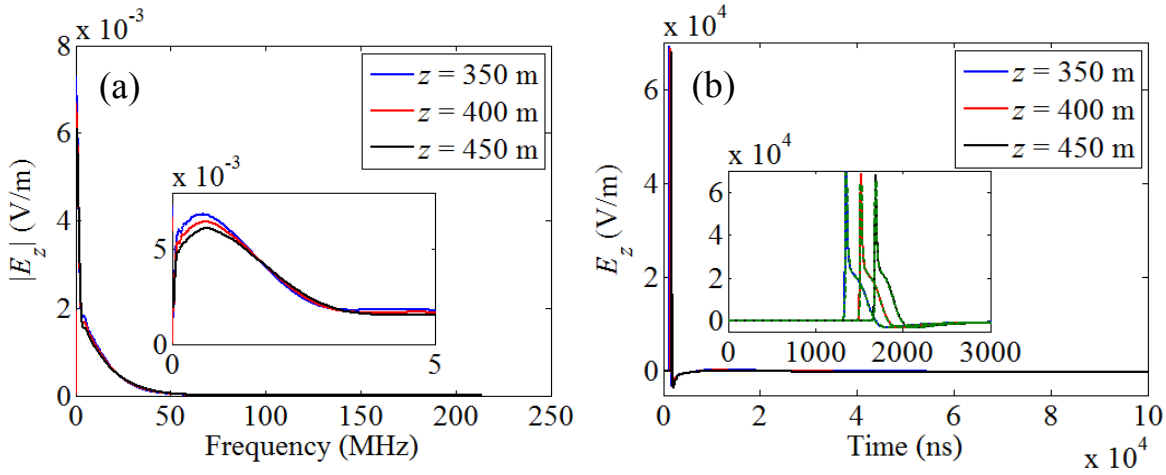

Figure 3. (a) The spectrum of the *z*-component of the electric field versus frequency. The inset shows a zoom at low frequencies. (b) We inverse Fourier transformed the spectrum to verify the time response in Figure 2. The dashed green lines in the inset showing a zoom at early times are the result of the inverse Fourier transform.

4. SIMULATION RESULTS FOR FINITE WIRES USING THE ATLOG MODEL

The parameters we take in this section on the simulations are as follows: lossy ground with $\varepsilon_4 = 10\varepsilon_0$ and $\sigma_4 = 0.0015\,\text{S/m}$ or PEC ground, $\varepsilon_2 = \varepsilon_0$ (i.e. no coating), $a = 1.27\,\text{cm}$, and $\sigma_0 = \dfrac{1}{R\pi a^2} = 2.9281\times10^7\ \text{S/m}$ using $R = 6.74\times10^{-5}\ \Omega/\text{m}$. We consider a 100 m long wire above ground with $h = 10\,\text{m}$. The finite line is left open-circuited at both ends. The air conductivity time dependence under the SREMP excitation is shown in Figure 4, but cannot be directly used in the frequency-domain ATLOG code. It is non zero only for a limited time when the pulse hits the structure; at any other time the air conductivity is basically zero (though the precise value is important as discussed later in this report). For this reason, we consider here two values of air conductivity: 0 and 0.07 S/m, and use this discretized (constant) input in the ATLOG simulation.

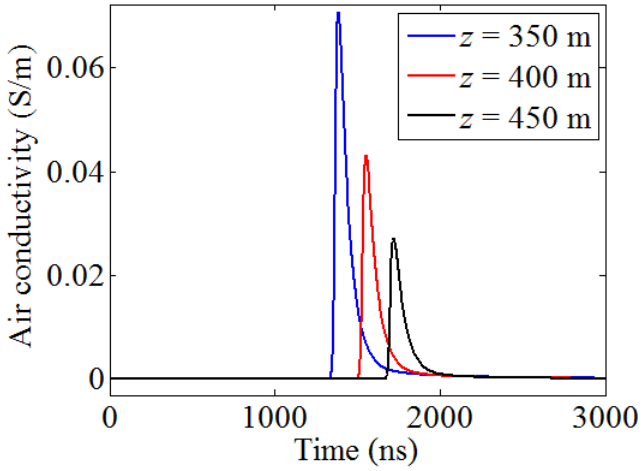

Figure 4. Air conductivity versus time at three positions along the wire.

The finite-wire formulation in Section 2 is here employed. We first perform an analysis to confirm proper frequency gridding for the excitation spectrum to achieve reasonable current data. Note that to correctly capture the early time of the current waveform, we needed to pad the electric field incident data with zeroes at late times as to have enough samples at low frequencies in its spectrum. Under the field drive shown in Section 3, the induced current in the middle of the line (i.e. 400 m) is given in Figure 5 for various ground and air conductivity conditions as described in the figure caption. One can see that for all cases, a frequency gridding of 333 Hz is sufficient for convergence of the current result both at early and late times. The upper frequency is taken from the time spacing as 214.14 MHz.

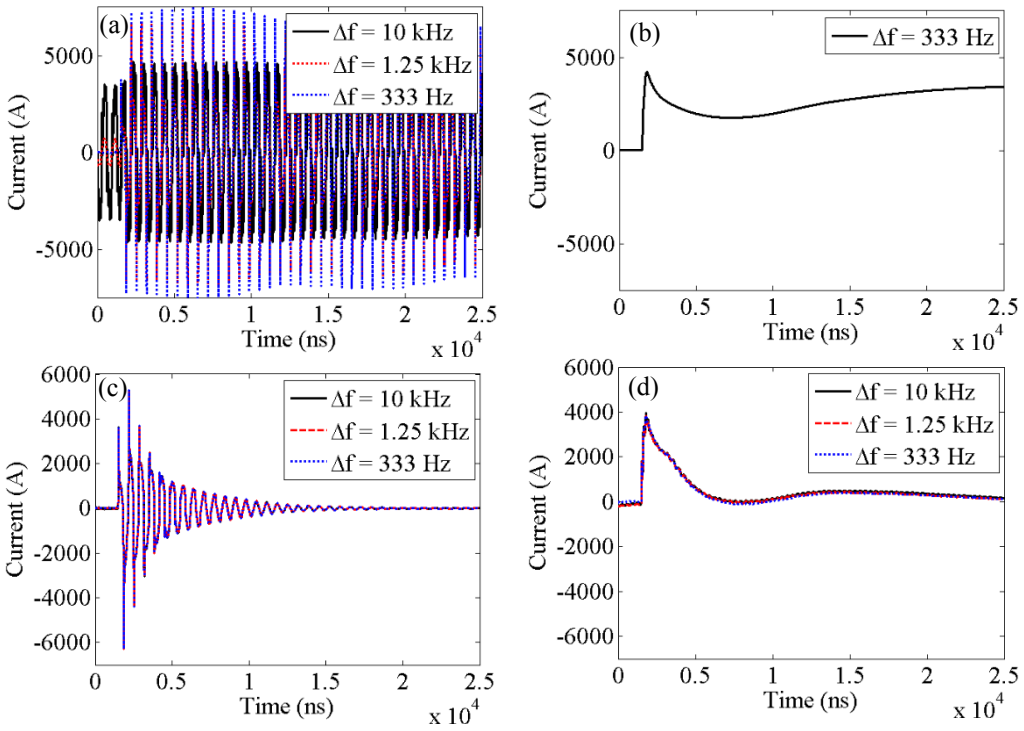

Figure 5. Current versus time for the SREMP excitation between 350 m and 450 m; results are based on the frequency-domain ATLOG model with various frequency sampling of the excitation field as indicated in the legends. (a) PEC ground, no air conductivity. (b) PEC ground, 0.07 S/m constant air conductivity. (c) Lossy ground, no air conductivity. (d) Lossy ground, 0.07 S/m constant air conductivity. The current is evaluated at 400 m.

We then refer to the results in Figure 5 with a frequency grid of 333 Hz. The delay between two peaks in Figures 5(a) and 5(c) should be $\Delta t = 200/c = 666.67\,\text{ns}$; the delay between two peaks there observed is equal to 675 ns, thus in good agreement. When no air conductivity is present, the initial peaks of the PEC ground case are slightly larger than the ones of the lossy ground case.

5. COMPARISON OF ATLOG TO XYCE (CIRCUIT SIMULATOR) RESULTS FOR FINITE WIRES

We employ in this section the circuit simulator Xyce [6, 7] under the SREMP excitation. While ATLOG can simulate lossy grounds and constant air conductivities, Xyce can analyze PEC grounds and time-varying air conductivities. To be able to compare ATLOG and Xyce results, the parameters we assume in the simulations are: PEC ground, $\varepsilon_2 = \varepsilon_0$ (i.e. no coating), $a = 1.27$ cm, and $\sigma_0 = \dfrac{1}{R\pi a^2} = 2.9281\times10^{7}$ S/m using $R = 6.74\times10^{-5}$ Ω/m, and constant air conductivity. We consider a 100 m long wire above ground with $h = 10$ m. The finite line is left open-circuited at both ends.

We thus compare in Figure 6 the ATLOG result for the case with PEC ground to the one computed by the circuit simulator Xyce assuming a wire located between either 350 m and 450 m, or 1500 m and 1600 m, or 3000 m and 3100 m. In ATLOG, we use a frequency gridding of 333 Hz. In both codes, we assume constant values of air conductivity: 3.44094×10^{-6} S/m for the line starting at 350 m, 2.7×10^{-7} S/m for the line starting at 1500 m, and 1.92×10^{-9} S/m for the line starting at 3000 m. Good agreement between the two codes is observed, especially for the response at early times. One can see that the closer to the nuclear-weapon event, the larger is the current induced at early times; moreover, the current decay is faster as the air exhibits larger air conductivity closer to the nuclear-weapon event.

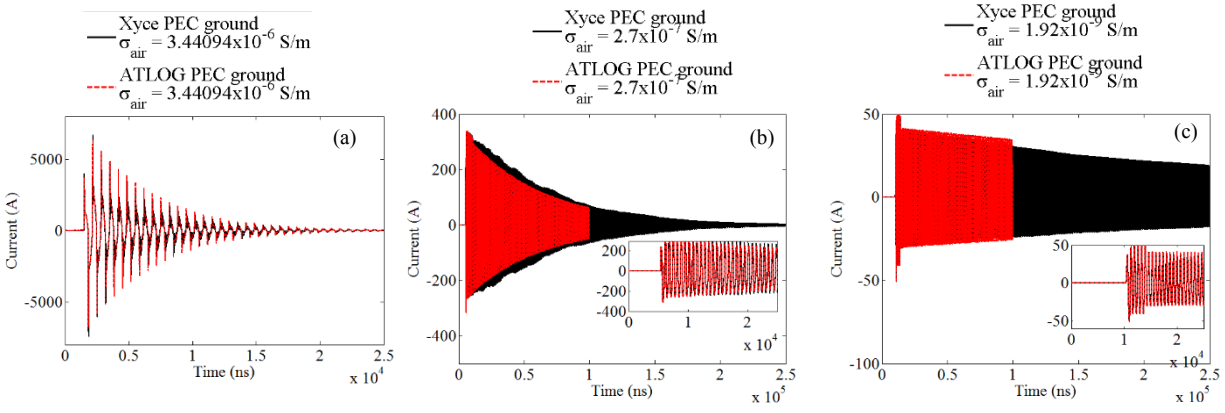

Figure 6. Current versus time for the SREMP excitation between (a) 350 m and 450 m, (b) 1500 m and 1600 m, and (c) 3000 m and 3100 m; results are based on the frequency-domain ATLOG model and Xyce with PEC ground and the constant air conductivity values indicated in the legends. The insets in (b) and (c) show zooms at early times. The current is evaluated at 400 m in (a), at 1560 m in (b) and at 3060 m in (c).

We then compare in Figure 7 the ATLOG results for the case with PEC ground with constant air conductivity of 4.7×10^{-7} S/m for the 100 m long wire starting at 1500 m to the one computed by the circuit simulator Xyce for the case with PEC ground and time-varying air conductivity for a

wire located between 1500 m and 1600 m. For the result in Figure 7, we have chosen in ATLOG the conductivity value at the time for which the current has decayed to $1/e$ of the peak value. Good agreement between the two codes is once again observed. For this particular case, a favorable comparison indicates that at these distances the time dependence of the air conductivity could be potentially approximated by a constant, average value of its decay around the tail of the time signal, for example the value of conductivity at a time where $1/e$ of the current peak is reached.

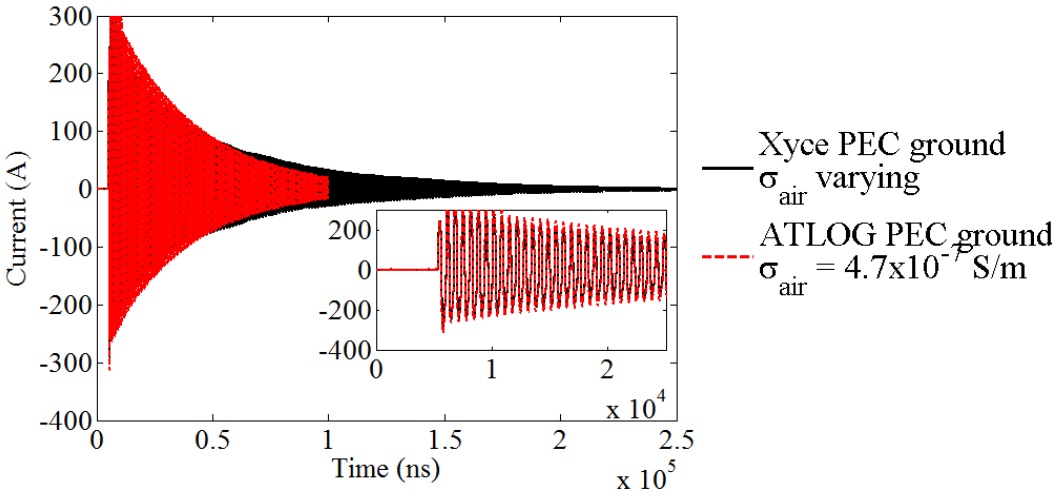

Figure 7. Current versus time for the SREMP excitation for a wire between 1500 m and 1600 m; results are based on the frequency-domain ATLOG model with PEC ground and constant air conductivity of 4.7×10^{-7} S/m and Xyce with PEC ground and time-varying air conductivity. The inset shows a zoom at early times. The current is evaluated at 1560 m.

Because the large air conductivity is present only for a limited amount of time as shown in Figure 4, we can use the frequency domain ATLOG code to account for an average, large air conductivity only during that time (e.g. the peak value of 0.07 S/m); then, when the air conductivity disappears, we use the current $I(z,t_0)$ at time t_0 to compute the behavior for $t \geq t_0$ as follows:

$$I(z,t) = \sum_{n=1}^{\infty} A_n \cos\{\omega_n'(t-t_0)\} e^{-\omega_n''(t-t_0)} \sin\left[n\pi\left(\frac{z-z_-}{z_+-z_-}\right)\right], \quad t \geq t_0 \tag{10}$$

with

$$A_n = \frac{2}{z_+-z_-}\int_{z_-}^{z_+} I(z,t_0)\sin\left[n\pi\left(\frac{z-z_-}{z_+-z_-}\right)\right]dz \tag{11}$$

and

$$\omega_n = \omega_n^{'} + j\omega_n^{''} \approx \frac{n\pi}{\sqrt{\mu_0 \bar{\varepsilon}_0}(z_+ - z_-)} \Big/ \sqrt{1 + \frac{\ln\left\{1 + e^{-j\pi/4}\sqrt{\frac{z_+ - z_-}{n\pi h^2 \sigma_4 \eta_0}}\right\}}{\operatorname{arccosh}(h/a)}} \tag{12}$$

with

$$\bar{\varepsilon}_0 = 8.854\times10^{-12} - j\frac{\sigma_0}{\frac{n\pi}{\sqrt{\mu_0 8.854\times10^{-12}}(z_+ - z_-)}} \tag{13}$$

to account for a constant, small air conductivity value σ_0 at later times (e.g. 0.0008 S/m).

The result of this operation is shown in Figure 8(a) for the wire on top of PEC ground and in Figure 8(b) for the wire on top of lossy ground. The former result is also compared to the one computed by Xyce using a time-varying air conductivity in Figure 8(a); good agreement is observed, even though only two values of air conductivities were used in the ATLOG model, whereas the full time dependence of the air conductivity as in Figure 4 was used in Xyce.

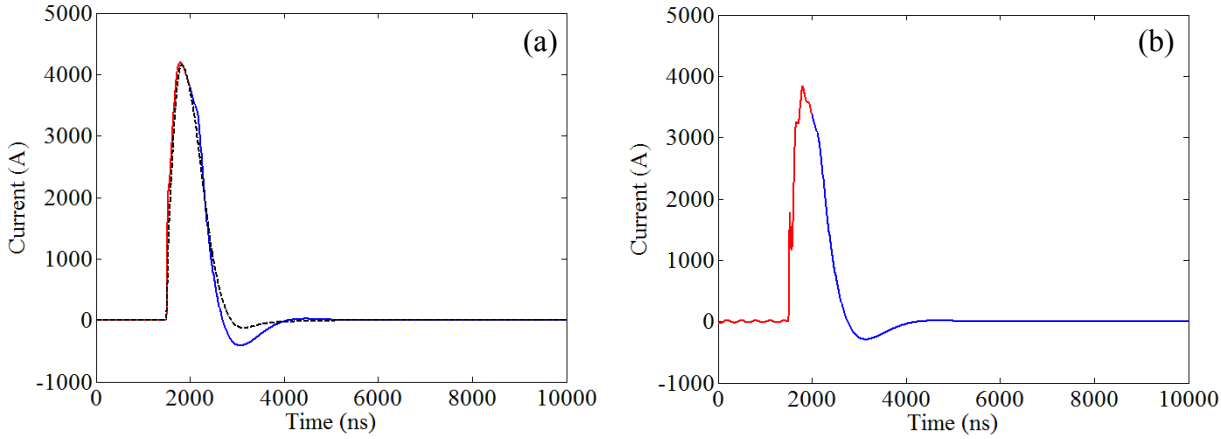

Figure 8. Current versus time for the SREMP excitation between 350 m and 450 m with (a) PEC ground and (b) lossy ground. Results are based on the frequency-domain ATLOG model with air conductivity of 0.07 S/m (red) and Eq. (10) using a constant air conductivity of 0.0008 S/m (blue). The black dashed curve in (a) is the result from Xyce using the time-varying air conductivity in Figure 4. The current is evaluated at 400 m.

However, because of the large conductivity values at earlier times, more analyses need to be performed to assess whether the results in Figure 8 are valid. This question stems from the fact that in the case where the air conductivity is large, the wire might not even see the ground --- in other words, the wire is immersed in an "air ground", as schematically reported in Figure 9. Moreover, if the air conductivity change progresses along the line at (or near) the wave propagation velocity, the detailed transition between the two conductivity states would be

difficult to capture with the two-state model described above; a time-domain ATLOG code would be required for further analyses. These two investigations will be carried out in future works.

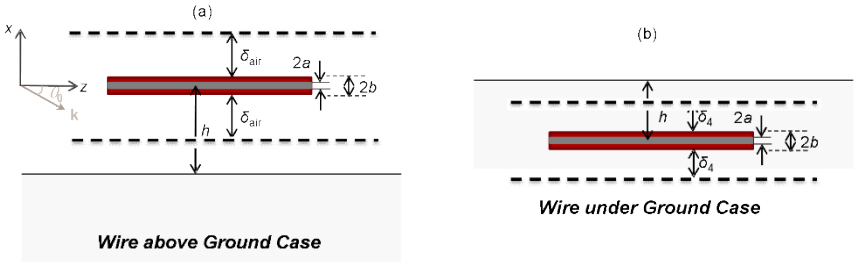

Figure 9. (a) Schematic representation of a wire above ground with air conductivity. If the air conductivity is large so that the skin depth is small, the wire will not see the ground, and could effectively be modeled using the same approach as implemented for a wire deeply under the ground as in panel (b).

6. CONCLUSIONS

In this report we computed results for the current induced on finite-length conductors interacting with a conducting ground when excited by the SREMP. We used the frequency-domain ATLOG model we developed in a previous work [2, 3] and compared these results to ones computed using the circuit simulator Xyce [6, 7]. Good agreement has been observed between the two models. The ATLOG model allows for the treatment of finite or infinite lossy, coated wires and lossy grounds. This capability in conjunction with the ability to treat a variety of different transmission-line scenarios (cable above ground, resting on the ground, and buried beneath the ground) makes our model general and a more of a complete tool for TL consequence assessment. The ATLOG method is offered as an alternative option to a full-wave solution, as opposed to a wholesale replacement method. It is our experience that this type of faster-running tool is extremely useful to quickly assess a wide variety of scenarios and determine relative impact over a wide parameter space. In addition, this type of tool may be of value because it does not necessarily require an expert user and, combined with other toolsets, can be used in an operator-mode for damage assessment.

REFERENCES

[1] S. W. White, P. P. Whalen, and A. R. Heath, “Source Calculations for the US-Japan Dosimetry Working Group”, 18 November 2001, LA-UR-01-6594.

[2] S. Campione, L. K. Warne, L. I. Basilio, C. D. Turner, K. L. Cartwright, and K. C. Chen, “Electromagnetic pulse excitation of finite- and infinitely-long lossy conductors over a lossy ground plane,” *Journal of Electromagnetic Waves and Applications* 31(2), 209-224, DOI: 10.1080/09205071.2016.1270776 (2017).

[3] L. K. Warne and K. C. Chen, "Long Line Coupling Models," *Sandia National Laboratories Report,* SAND2004-0872, Albuquerque, NM, 2004.

[4] C. D. Turner, M. F. Pasik, D. B. Seidel, T. D. Pointon, and K. L. Cartwright, "EMPHASIS/Nevada UTDEM User Guide Version 2.1.1," *Sandia National Laboratories Report,* vol. SAND2014-16735, pp. Albuquerque, NM, 2014.

[5] CST Microwave Studio, https://www.cst.com/products/cstmws – 2017.

[6] https://xyce.sandia.gov

[7] E. R. Keiter, H. K. Thornquist, R. J. Hoekstra, T. V. Russo, R. L. Schiek and E. L. Rankin, "Parallel transistor-level circuit simulation," in *Advanced Simulation and Verification of Electronic and Biological Systems*, P. Li, L. M. Silveira, and P. Feldmann, Eds. New York, NY: Springer, 2011, ch. 1, pp. 1-21.

DISTRIBUTION

Number	Mail Stop	Name	Dept.
1 (electronic)	MS0492	K. C. Chen	0411
1 (electronic)	MS0899	Technical Library	9536
1 (electronic)	MS1152	G. Pena	1350
3	MS1152	S. Campione	1352
3	MS1152	L. K. Warne	1352
3	MS1152	L. I. Basilio	1352
1 (electronic)	MS1152	S. Campione	1352
1 (electronic)	MS1152	L. K. Warne	1352
1 (electronic)	MS1152	L. I. Basilio	1352
1 (electronic)	MS1152	K. L. Cartwright	1352
1 (electronic)	MS1152	K. Sainath	1352
1 (electronic)	MS1168	L. X. Schneider	1350
1 (electronic)	MS1173	L. D. Bacon	5443
1 (electronic)	MS1173	M. J. Walker	5443
1 (electronic)	MS1177	R. L. Schiek	1355
1 (electronic)	MS1177	J. P. Castro	1355
1 (electronic)	MS1189	R. B. Campbell	1641
1 (electronic)	MS9007	C. Lam	8115


Sandia National Laboratories